Murdock, D., Harris, S. J., Clark, I. P., Greetham, G. M., Towrie, M., Orr-Ewing, A. J., & Ashfold, M. N. R. (2015). UV-Induced Isomerization Dynamics of N-Methyl-2-pyridone in Solution. Journal of Physical Chemistry A, 119(1), 88-94. 10.1021/jp511818k

UV-Induced Isomerization Dynamics of *N*-Methyl-2-Pyridone in Solution

Daniel Murdock,[1]* Stephanie J. Harris,[1] Ian P. Clark,[2] Gregory M. Greetham,[2] Michael Towrie,[2] Andrew J. Orr-Ewing,[1] and Michael N. R. Ashfold[1]

[1] School of Chemistry, University of Bristol, Cantock's Close, Bristol, BS8 1TS, United Kingdom.

[2] Central Laser Facility, Research Complex at Harwell, Science and Technology Facilities Council, Rutherford Appleton Laboratory, Didcot, Oxfordshire, OX11 0QX, United Kingdom

Abstract

The photoisomerization dynamics of *N*-methyl-2-pyridone (NMP) dissolved in CH_3CN have been interrogated by time-resolved electronic and vibrational absorption spectroscopy. Irradiation at 330 or 267 nm prepares NMP(S_1) molecules with very different levels of vibrational excitation, which rapidly relax to low vibrational levels of the S_1 state. Internal conversion with an associated time constant of 110(4) ps, leading to reformation of NMP(S_0) molecules, is identified as the dominant (>90%) decay pathway. Much of the remaining fraction undergoes a photo-initiated rearrangement to yield two ketenes (revealed by their characteristic antisymmetric C=C=O stretching modes at 2110 and 2120 cm^{-1}), which are in equilibrium. The rate of this isomerization is found to be pump-wavelength dependent, consistent with *ab initio* electronic structure calculations which predict a barrier on the S_1 potential energy surface *en route* to a prefulvenic conical intersection, by which isomerization is deduced to occur. Two kinetic models – differentiated by whether product branching is deduced to occur in the S_1 or S_0 electronic

states – are presented and used with nearly equal success in the analysis of the experimental data, highlighting the difficulties associated with deducing mechanistic information from kinetic data alone.

TOC Graphic

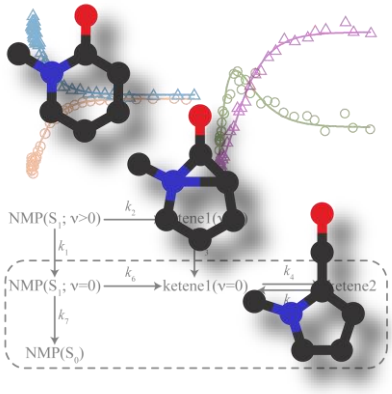

Keywords

Ultrafast pump-probe spectroscopy

Kinetics

Solution-phase photochemistry

Photoisomerization

INTRODUCTION

The structural changes induced in molecules by absorption of ultraviolet (UV) radiation constitute an important topic in chemistry and biology.[1,2] Many biologically relevant molecules, most notably the DNA bases, have evolved in such a way that their excited-state chemistry is dominated by internal conversion (IC) to the ground (S_0) electronic state,[3] thereby minimizing the potentially catastrophic effects of photodissociation or photoisomerization. In contrast, considerable attention has been devoted to designing molecules that can act as photoswitches, where a UV photoinduced change is both reversible and occurs with a high quantum yield.[4] Numerous examples of photoinduced unimolecular reactions can be found in the literature, ranging from bond fission[5] and hydrogen-atom transfer processes,[6,7] to cis-trans isomerization reactions in proteins.[8,9] The making and breaking of bonds occurs on femtosecond to picosecond timescales,[10] and can thus be followed in real time using time-resolved spectroscopic techniques.

Here we report the application of transient electronic (TEA) and vibrational (TVA) absorption spectroscopy to investigate the UV-induced photochemistry of N-methyl-2-pyridone (NMP) following excitation at two different wavelengths: 330 and 267 nm. NMP consists of a 6-membered heterocyclic ring with a carbonyl group α to the nitrogen atom and as such is particularly well suited to mechanistic interrogation using IR methods. The carbonyl and amide stretch modes around 1600 cm^{-1} provide convenient markers for the parent molecule population, while any ketene products (a potential result of photoinduced isomerizations) should be observable *via* their characteristic C=C=O antisymmetric stretch mode around 2100 cm^{-1}. The appearance of such ketene stretch

features has been used successfully as evidence for photoisomerization in several previous ultrafast spectroscopic investigations.[11-14] Combining the present experimental findings with the results of complementary *ab initio* calculations provides new and detailed insights into the decay pathways available to NMP(S_1) molecules. The present study also provides a chastening reminder of the limits to which we can unambiguously establish mechanistic details simply by kinetic modelling and estimating selected product yields, however – even when, as here, one is able to call on transient electronic *and* vibrational spectroscopy measurements and *ab initio* electronic structure calculations.

EXPERIMENTAL AND COMPUTATIONAL METHODLOGY

The TEA (267 nm pump) and TVA (267 and 330 nm pump) spectra were recorded using the ULTRA laser facility at the Rutherford Appleton Laboratory,[15] while the 330 nm pump TEA experiments were performed at the University of Bristol.[16] In both cases, an amplified titanium sapphire laser system generated 800 nm (band center) pulses with 50 fs (35 fs at Bristol) pulse duration and 10 kHz (1 kHz) repetition rate. A portion of this light was used to generate the UV pump radiation either through frequency tripling (267 nm) or *via* a tunable optical parametric amplifier (330 nm). The broadband UV/visible probe used in the TEA experiments was produced by focusing a portion of the 800 nm output into a CaF_2 disc, while a further portion of this light was used to pump an optical parametric amplifier to generate the mid-IR probe radiation (~500 cm^{-1} bandwidth) used in the TVA experiments. In each experiment the pump and probe pulses were overlapped in the sample with their linear polarization vectors aligned at the magic angle, before the transmitted radiation was dispersed by a grating onto a 128 element

mercury cadmium telluride array detector (TVA) or onto a 512 element silicon array (TEA). NMP and CH_3CN were obtained from Sigma-Aldrich and used without further purification. The samples were flowed continuously through a Harrick cell with a 100 μm PTFE spacer between CaF_2 windows (a 380 μm spacer was used for the 330 nm pump TEA experiment), and the 60 mM solution concentrations were chosen to ensure an absorbance, *A* ~0.5 at 267 nm. The ground state equilibrium structures of NMP and two plausible ketene structures, and their respective anharmonic vibrational wavenumbers were calculated using Gaussian09.[17] So, too, was the geometry of a prefulvenic conical intersection between the S_1 and S_0 potential energy surfaces (PESs). Cuts through the *ab initio* S_1 and S_0 PESs linking the equilibrium structure of NMP(S_0) with this conical intersection geometry were constructed using Molpro2010.1.[18] and the linearly interpolated internal coordinates (LIIC) methodology.[19]

RESULTS AND DISCUSSION

Transient absorption measurements

Figure 1(a) displays selected TEA spectra obtained by pumping a 60 mM NMP/CH_3CN sample at 267 nm and setting the broadband probe to cover the 350-625 nm region. This pump wavelength excites the blue edge of the S_1–S_0 absorption band of NMP (the static UV/visible absorption spectrum of NMP is included in the supporting information (SI)). At small Δt, there are two positive (henceforth termed gain) signals, one peaking around 480 nm and extending to λ_{Probe}>650 nm, and the other maximizing at λ_{Probe}<350 nm. These features are present at the earliest time delays probed, and decay on an ~100 ps timescale. We assign them to absorptions from the S_1 state. The spectral

width of these features decreases with increasing Δt, indicative of vibrational cooling of these S_1 molecules.[2] A negative (henceforth termed bleach) feature is also present, centered around 375 nm. Since the UV/visible absorption band of NMP does not extend this far to the red, this feature is assigned to stimulated emission from the S_1 electronic state. As with the gain signals, the stimulated emission band appears to both shift and narrow as time progresses, though we recognize that these apparent changes could simply be an artifact caused by the extensive overlap with the gain features.

Figure (1b) shows selected TVA spectra obtained by pumping NMP at 267 nm and probing the 1520–1720 cm^{-1} range. This region covers the amide and carbonyl stretch motions of the parent molecule, and thus provides a spectral window in which the parent concentration can be monitored as a function of Δt. Four bleach features are evident, centered around 1545, 1590, 1600, and 1665 cm^{-1}. These features are seen to recover with increasing Δt, but the recovery is incomplete – asymptotically reaching ~90% – indicating that ~10% of the initially excited molecules evolve to photoproducts. Gain signals located to the low wavenumber side of the bleaches are also present at early times, each demonstrating the spectral narrowing and shift to higher wavenumber characteristic of vibrational cooling.[2,20,21] The long-lived nature of the S_1 state (fig. 1(a)) implies that these evolving gain signals are more likely attributable to vibrationally excited S_1 (rather than S_0) molecules.

Moving the probe region to span the 2050–2150 cm^{-1} range allows us to monitor the buildup of any ketene product molecules. The ~90% recovery of the parent bleach

features indicates that any product formation must be a minor reaction channel. Nonetheless, as figure 1(c) shows, 267 nm excitation of NMP does indeed give rise to an observable ketene signal. Due to the combination of extremely low signal levels (<25 μOD) and the highly vibrationally excited nature of the ketene products at short pump-probe delays, the earliest time any signal is observable is $\Delta t \approx 5$ ps. Closer inspection of the later time traces in figure 1(c) suggests that there are actually *two* ketene features: a peak at ~2110 cm^{-1} (henceforth assigned as ketene1), which reaches its maximum intensity after ~40 ps before decreasing in magnitude, and a second peak at ~2120 cm^{-1} (ketene2) which grows over the entire range of pump-probe time delays sampled. A weak bleach signal located at 2070 cm^{-1} also grows in at later times, although the presence of overlapping ketene structure could potentially be hiding any early time signal. Comparison with the FTIR spectrum of neat CH_3CN reveals that this is a solvent band.

The 60 mM NMP/CH_3CN solutions were also pumped at 330 nm – *i.e.* at the red-edge of the S_1–S_0 absorption band – with transient absorption spectra obtained by probing the 350–625 nm, 1520–1720 cm^{-1}, and 2050–2150 cm^{-1} regions. These data are shown in figures 2(a)–2(c), respectively. Overall, the λ_{Pump}=330 nm spectra closely resemble those recorded at λ_{Pump}=267 nm, with the major difference being the much reduced vibrational excitation revealed by the NMP(S_1) and ketene product features. Within our signal to noise level, the vibrationally-hot ketene signal is essentially absent. This decrease in vibrational energy content at early times follows naturally from the reduction in energy available to the molecules following photoexcitation.

The substantial spectral overlap between bands attributed to ketene1 and ketene2 in figures 1(c) and 2(c), and the vibrationally hot NMP(S_1) and the NMP(S_0) bleach signals in figure 1(b) requires fitting in terms of model functions to extract the time-dependent populations needed for a kinetic analysis. A brief overview of the fitting procedures used in the analysis of these datasets and representative decompositions are included in the SI. For all other spectral features, numerical integration over the regions of interest was used to extract the required information. The results of these analyses are shown in figures 3(a) and (b) for λ_{Pump}=330 nm, and figures 4(a) and (b) for λ_{Pump}=267 nm.

Several features of the kinetic traces shown in figures 3 and 4 merit note: (i) the buildup of vibrationally-relaxed ketene1 (dark blue circles) is faster in figure 4(b) than in figure 3(b), indicating a pump wavelength dependent reaction rate. (ii) The ketene2 signal (light blue triangles) grows as that associated with ketene1 decays, but the ketene1 signal never falls to zero; instead an equilibrium is formed with ketene2. (iii) There is an ~20 ps induction period before the NMP(S_0) bleach (dark blue circles) begins to recover (shown more clearly in the SI). This delay is attributed to the ~100 ps S_1 lifetime and subsequent vibrational cooling after radiationless transfer to highly excited levels of the S_0 state.[14,21]

Kinetic modeling

The TEA and TVA experimental data may be fit equally well with (at least) two kinetic models, differentiated by whether the branching between reforming NMP(S_0,v=0) molecules or forming ketene products is assumed to occur before or after radiationless

transfer to the S_0 potential energy surface. The former (which we term Scheme A) is guided by the computational studies of Barbatti *et al.*,[22] which located a number of conical intersections linking the S_1 and S_0 PESs of the closely related 2-pyridone molecule that could be accessed by appropriate out-of-plane ring puckering motions. This model encourages fitting the present TVA and TEA data according to the following kinetic scheme:

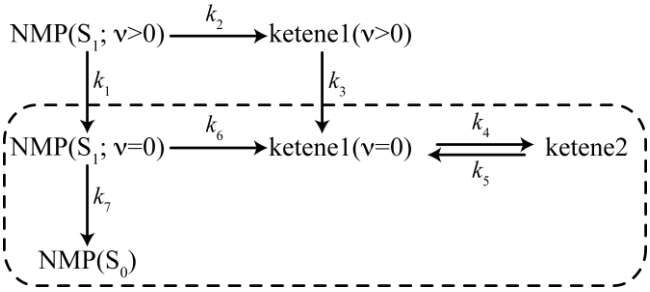

Scheme A

k_7 denotes the rate coefficient for IC from thermalized NMP(S_1) molecules (henceforth represented as NMP(S_1;ν=0)) to highly vibrationally excited ground state levels (S_0;ν>>0). Subsequent vibrational cooling within the S_0 manifold is assumed to be much faster than IC and thus have minimal impact on the observed rate coefficient. k_1 and k_3 are the vibrational cooling rate coefficients for NMP(S_1;ν>0) and ketene1(ν>0), respectively, k_2 and k_6 are the rate coefficients for isomerization from NMP(S_1;ν>0) and NMP(S_1;ν=0), respectively, while k_4 and k_5 are the coefficients controlling the equilibrium between ketene1 and ketene2. Scheme A allows only two active decay pathways for the photoprepared S_1 molecules: IC to repopulate the S_0 state and isomerization to the ketene species (neglecting any other potential photoreactions such as N–CH_3 bond fission), and assumes that these occur via separate conical intersections.

The two pump wavelengths employed in the present investigation excite different regions of the NMP absorption band. 267 nm excitation prepares NMP(S_1;v>0) molecules, whereas the 330 nm pump radiation excites much closer to the origin of the S_1–S_0 transition. If we make the simplifying assumption that λ_{Pump}=330 nm prepares NMP(S_1;v=0) molecules exclusively, then the kinetic scheme reduces to the part contained within the dashed box. Depending upon whether NMP(S_1;v>0) or NMP(S_1;v=0) is populated initially, analytical solutions for the time-dependent populations for all species of interest may then be obtained.[23]

The solid lines in figures 3(a) and (b) are fits to the reduced kinetic model applicable to the λ_{Pump}=330 nm data. The best-fit rate coefficients and corresponding time constants are collated in Table 1, where the numbers in parentheses represent the one standard deviation uncertainty in the last significant digit(s). In order to extract values for k_4 and k_5, the relative band intensities for ketene1 and ketene2 need to be known. In the absence of this information, we have assumed a ratio of 1:1 – broadly consistent with the results of the present anharmonic wavenumber calculations (see SI) which predict antisymmetric C=C=O stretch band intensities for ketene1 and ketene2 of 323 km mol^{-1} and 354 km mol^{-1}, respectively.

The values for k_6 and k_7 obtained from the fit of the λ_{Pump}=330 nm data were subsequently used as non-adjustable parameters when fitting the λ_{Pump}=267 nm data to the full kinetic model. Experimentally, we do not have access to the NMP(S_1;v>0) molecules prepared by 267 nm excitation (these are expected to lose much of their excess

vibrational energy quicker than the ~1 ps experimental time response). Consequently, the value for k_1 used in the fit is set to >1 ps^{-1}, with k_2 being constrained to equal $0.05 \times k_1$. This constraint is required to reproduce the ~90% repopulation of the parent S_0 state. Changing k_1 is found to have little effect on the values of the other rate coefficients, although reducing it can induce an early-time build-up of population in the model kinetic trace for NMP(S_1;v=0). The results of this fit are depicted as solid lines in figures 4(a) and 4(b), with the best-fit rate coefficients given in Table 1. The fit demonstrates that the constrained kinetic model described by scheme A can successfully account for all of the present experimental observations.

The results in Table 1 combined with the ~90% bleach recovery observed in figures 1(b) and 2(b) highlight that the photophysics of NMP(S_1) is dominated by IC to the S_0 state. Reaction to form ketene1 and ketene2 (or any other undetected products) is a minor pathway, as indicated by the ~2 ns isomerization time constant obtained for NMP(S_1;v=0). This slow rate, together with the observed λ_{Pump} dependence, is reminiscent of the kinetics measured for S–CH_3 bond cleavage in thioanisole[24] and *p*-methylthioanisole,[25,26] and hints at the presence of a potential barrier hindering reaction. Unfortunately, the lack of an experimental value for k_2 prevents our drawing any quantitative conclusions about the λ_{Pump} dependence from the present results. We note that the ratio of the two ketene products also appears to be λ_{Pump} dependent.

As noted previously, we can also envisage a decay mechanism (scheme B) where all of the NMP(S_1) population passes through a single conical intersection. In contrast to

scheme A, scheme B assumes that the ~100 ps S_1 lifetime reflects the time taken to reach (and pass through) this conical intersection, and that the topology determines the branching between reforming NMP(S_0;ν=0) molecules or of forming ketene1 and ketene2. The alternative kinetic scheme appropriate for 330 nm excitation (*i.e.* the analogue of the part of scheme A bounded by the dashed box) is:

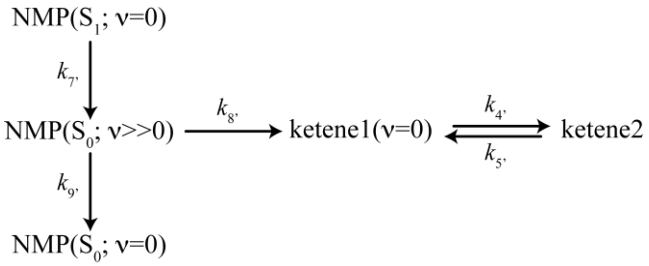

Scheme B

where $k_{7'}$ denotes the rate coefficient for $S_1 \rightarrow S_0$ IC, $k_{8'}$ and $k_{9'}$ are the rate coefficients controlling formation of ketene1 and vibrational cooling to NMP(S_0;ν=0), respectively, and $k_{4'}$ and $k_{5'}$ are the equilibrium coefficients. As before, we assume that 330 nm excitation prepares NMP(S_1;ν=0) molecules exclusively and that ketene1 and ketene2 have identical band intensities. In this fitting of the data, $k_{9'}$ is fixed at 0.1 ps^{-1} ($\tau_{9'}$ = 10 ps) – a typical vibrational cooling rate for a polyatomic molecule in solution in CH_3CN.[14,25] The dashed curves in figure 3(a) and 3(b) illustrate the quality of the fit to the λ_{Pump} = 330 nm data assuming scheme B and the best-fit rate coefficients listed in Table 2.

Clearly, both kinetic schemes are able to provide essentially identical quality fits to the data, despite the significantly different ketene formation time constants (~2 ns in

scheme A, *cf*. ~200 ps when using scheme B). Indeed, the two models return almost identical IC rate coefficients (k_7 in scheme A, $k_{7'}$ in scheme B) and equilibrium coefficients (k_4 and k_5 in scheme A, $k_{4'}$ and $k_{5'}$ in scheme B). These results suggest that schemes A and B should probably both be recognized as limiting models for the true relaxation/reaction dynamics following near UV photoexcitation of NMP. However, they also serve to re-emphasize the challenges associated with modeling and interpreting the multidimensional relaxation dynamics of polyatomic systems when armed with only a limited set of experimental observations.

Ab initio calculations

Plausible structures for ketene1 and ketene2 are shown in figure 5. Both structures arise through contraction of the 6-membered ring, forming a 5-membered heterocycle with a pendant ketene functional group. The two structures are related by a [1,3]-hydrogen atom shift, and are predicted to be near isoenergetic at the MP2/6-311+G(*d*,*p*) level of theory. The anharmonic wavenumber predictions for the antisymmetric C=C=O stretching motions are in excellent agreement with the experimentally observed values (see SI). A possible route to these isomerization products involves passing through the prefulvene type conical intersection shown in figure 5, calculated using the complete active space self consistent field method with an active space of eight electrons in seven orbitals (CASSCF(8,7)) and a reduced 6-31G(*d*) basis set. The S_0 and S_1 potential energy curves shown in figure 5 were calculated along the LIIC linking the equilibrium structure of NMP(S_0) with this conical intersection geometry. The S_1 potential estimated in this way exhibits a large (~3 eV) energy barrier along the LIIC path. Since the LIIC approach

used here will not yield the minimum energy reaction path, the magnitude of the reported barrier must be regarded very much as an upper limit. Nonetheless, the prediction of an energy barrier accords with the experimental observations of hindered isomerization from NMP(S_1;v=0) and of an increased isomerization rate upon decreasing λ_{Pump}.

CONCLUSIONS

TVA and TEA spectroscopies have been used to investigate the UV-induced photochemistry of N-methyl-2-pyridone in solution in CH_3CN. At both λ_{Pump}=330 nm and λ_{Pump}=267 nm, IC with an associated time constant of ~100 ps is the dominant (>90%) decay pathway, confirming the relative photostability inherent to many nitrogen-containing heterocycles.[3] However, a fraction of the photoexcited molecules react, forming two ketenes which are in equilibrium. The rate coefficient for this isomerization reaction is seen to increase with decreasing pump wavelength. Complementary *ab initio* calculations predict a prefulvenic conical intersection, with the C=O group out of the plane defined by the other five heavy atoms, linking the global S_1 and S_0 PESs. The structure of this conical intersection suggests that the isomerization proceeds via ring-contraction, with the two possible ketene products being linked by a [1,3] H-atom shift. The calculated cut through the S_1 PES shows a potential barrier *en route* to this conical intersection. This barrier must hinder reaction – consistent with the experimental observations of a slow, λ_{Pump} dependent, isomerization rate – but we stress that we have not attempted to calculate the true minimum energy pathway. Neither have we sought to locate any other conical intersections linking the S_1 and S_0 PESs that (by analogy with studies of the related molecule 2-pyridone)[22] must be present in this system, but the

finding that the S_1 state has a ~100 ps lifetime indicates that the pathways to all of them from the S_1 minimum have an associated potential barrier. We end with a note of caution: the present study is able to call on more complementary data (from both TEA and TVA spectroscopy measurements and from *ab initio* electronic structure calculations) than many condensed phase photochemistry studies, yet the kinetic modeling and product yield estimates are still insufficient to allow unambiguous distinction between two possible reaction mechanisms.

ASSOCIATED CONTENT

Static FTIR and UV/visible spectra of NMP/CH_3CN. Details and example fits from the decomposition procedures used in the extraction of kinetic traces shown in figures 3(b), 4(a) and 4(b). Expanded view of the early time S_0 bleach recovery. Calculated anharmonic wavenumbers for the parent NMP and ketene product molecules. Active space used in the construction of the LIIC PECs. This material is available free of charge *via* the Internet at http://pubs.acs.org.

CORRESPONDING AUTHOR

*(D.M.) E-mail: Daniel.Murdock@bristol.ac.uk; tel. +44(0)1179288312

Notes

The authors declare no competing financial interest.

ACKNOWLEDGEMENTS

This work was supported by the European Research Council through ERC Advanced Grant 290966 CAPRI and by EPSRC *via* Programme Grants EP/G00224X. We acknowledge STFC for programme access to the ULTRA laser facility (STFC Facility Grant ST/501784). SJH is grateful to the University of Bristol for a Postgraduate Research Scholarship. The authors thank Dr. T.N.V. Karsili for suggesting a prefulvenic form for the conical intersection.

(1) Nibbering, E. T. J.; Fidder, H.; Pines, E. Ultrafast Chemistry: Using Time-Resolved Vibrational Spectroscopy for Interrogation of Structural Dynamics. *Annu. Rev. Phys. Chem.* **2005**, *56*, 337–367.
(2) Rosspeintner, A.; Lang, B.; Vauthey, E. Ultrafast Photochemistry in Liquids. *Annu. Rev. Phys. Chem.* **2013**, *64*, 247–271.
(3) Crespo-Hernández, C. E.; Cohen, B.; Hare, P. M.; Kohler, B. Ultrafast Excited-State Dynamics in Nucleic Acids. *Chem. Rev.* **2004**, *104*, 1977–2019.
(4) Renth, F.; Siewertsen, R.; Temps, F. Enhanced Photoswitching and Ultrafast Dynamics in Structurally Modified Photochromic Fulgides. *International Reviews in Physical Chemistry* **2013**, *32*, 1–38.
(5) Ashfold, M. N. R.; King, G. A.; Murdock, D.; Nix, M. G. D.; Oliver, T. A. A.; Sage, A. G. πσ* Excited States in Molecular Photochemistry. *Phys. Chem. Chem. Phys.* **2010**, *12*, 1218–1238.
(6) Elsaesser, T.; Kaiser, W. Visible and Infrared Spectroscopy of Intramolecular Proton Transfer Using Picosecond Laser Pulses. *Chem. Phys. Lett.* **1986**, *128*, 231–237.
(7) Meech, S. R. Excited State Reactions in Fluorescent Proteins. *Chem. Soc. Rev.* **2009**, *38*, 2922.
(8) Gai, F.; Hasson, K. C.; McDonald, J. C.; Anfinrud, P. A. Chemical Dynamics in Proteins: the Photoisomerization of Retinal in Bacteriorhodopsin. *Science* **1998**, *279*, 1886–1891.
(9) Wand, A.; Gdor, I.; Zhu, J.; Sheves, M.; Ruhman, S. Shedding New Light on Retinal Protein Photochemistry. *Annu. Rev. Phys. Chem.* **2013**, *64*, 437–458.
(10) Zewail, A. H. Laser Femtochemistry. *Science* **1988**, *242*, 1645–1653.
(11) Laimgruber, S.; Schreier, W. J.; Schrader, T.; Koller, F.; Zinth, W.; Gilch, P. The Photochemistry of *o*-Nitrobenzaldehyde as Seen by Femtosecond Vibrational Spectroscopy. *Angew. Chem. Int. Ed.* **2005**, *44*, 7901–7904.
(12) Schmierer, T.; Schreier, W. J.; Koller, F. O.; Schrader, T. E.; Gilch, P. Impact of Vibrational Excitation on the Kinetics of a Nascent Ketene. *Phys. Chem. Chem. Phys.* **2009**, *11*, 11596–11607.
(13) Burdzinski, G.; Kubicki, J.; Sliwa, M.; Réhault, J.; Zhang, Y.; Vyas, S.; Luk, H. L.; Hadad, C. M.; Platz, M. S. Mechanistic Aspects of Ketene Formation Deduced From Femtosecond Photolysis of Diazocyclohexadienone, *o*-Phenylene Thioxocarbonate, and 2-Chlorophenol. *J. Org. Chem.* **2013**, *78*, 2026–2032.
(14) Murdock, D.; Harris, S. J.; Luke, J.; Grubb, M. P.; Orr-Ewing, A. J.; Ashfold, M. N. R. Transient UV Pump-IR Probe Investigation of Heterocyclic Ring-Opening Dynamics in the Solution Phase: the Role Played by nσ* States in the Photoinduced Reactions of Thiophenone and Furanone. *Phys. Chem. Chem. Phys.* **2014**, *16*, 21271–21279.
(15) Greetham, G. M.; Burgos, P.; Cao, Q.; Clark, I. P.; Codd, P. S.; Farrow, R. C.; George, M. W.; Kogimtzis, M.; Matousek, P.; Parker, A. W.; et al. ULTRA: a Unique Instrument for Time-Resolved Spectroscopy. *Appl. Spectrosc.* **2010**, *64*, 1311–1319.
(16) Roberts, G. M.; Marroux, H.; Grubb, M. P.; Ashfold, M. N. R.; Orr-Ewing, A. J. On the Participation of Photo-Induced N–H Bond Fission in Aqueous Adenine at 266 and 220 Nm: a Combined Ultrafast Transient Electronic and Vibrational

Absorption Spectroscopy Study. *J. Phys. Chem. A* **2014**, 141008135923005.
(17) Frisch, M. J.; Trucks, G. W.; Schlegel, H. B.; Scuseria, G. E.; Robb, M. A.; Cheeseman, J. R.; Scalmani, G.; Barone, V.; Mennucci, B.; Petersson, G. A.; et al. Gaussian 09, Revision D.01. *Gaussian 09, Revision D.01, Gaussian, Inc., Wallingford CT* **2013**.
(18) Werner, H.-J.; Knowles, P. J.; Lindh, R.; Manby, F. R.; Schütz, M.; Celani, P.; Korona, T.; Mitrushenkov, A.; Rauhut, G.; Adler, T. B.; et al. MOLPRO, Version 2010.1, a Package of Ab Initio Programs, 2010.
(19) Perun, S.; Sobolewski, A. L.; Domcke, W. Ab Initio Studies on the Radiationless Decay Mechanisms of the Lowest Excited Singlet States of 9H-Adenine. *J. Am. Chem. Soc.* **2005**, *127*, 6257–6265.
(20) Owrutsky, J. C.; Raftery, D.; Hochstrasser, R. M. Vibrational Relaxation Dynamics in Solutions. *Annu. Rev. Phys. Chem.* **1994**, *45*, 519–555.
(21) Hamm, P.; Ohline, S. M.; Zinth, W. Vibrational Cooling After Ultrafast Photoisomerization of Azobenzene Measured by Femtosecond Infrared Spectroscopy. *J. Chem. Phys.* **1997**, *106*, 519–529.
(22) Barbatti, M.; Aquino, A. J. A.; Lischka, H. Theoretical Investigation of the Mode-Specific Induced Non-Radiative Decay in 2-Pyridone. *Chemical Physics* **2008**, *349*, 278–286.
(23) Berberan-Santos, M. N.; Martinho, J. M. G. The Integration of Kinetic Rate Equations by Matrix Methods. *J. Chem. Educ.* **1990**, *67*, 375–379.
(24) Roberts, G. M.; Hadden, D. J.; Bergendahl, L. T.; Wenge, A. M.; Harris, S. J.; Karsili, T. N. V.; Ashfold, M. N. R.; Paterson, M. J.; Stavros, V. G. Exploring Quantum Phenomena and Vibrational Control in σ* Mediated Photochemistry. *Chem. Sci.* **2013**, *4*, 993–1001.
(25) Murdock, D.; Harris, S. J.; Karsili, T. N. V.; Greetham, G. M.; Clark, I. P.; Towrie, M.; Orr Ewing, A. J.; Ashfold, M. N. R. Photofragmentation Dynamics in Solution Probed by Transient IR Absorption Spectroscopy: πσ*-Mediated Bond Cleavage in *p*-Methylthiophenol and *p*-Methylthioanisole. *J. Phys. Chem. Lett.* **2012**, *3*, 3715–3720.
(26) Harris, S. J.; Murdock, D.; Zhang, Y.; Oliver, T. A. A.; Grubb, M. P.; Orr Ewing, A. J.; Greetham, G. M.; Clark, I. P.; Towrie, M.; Bradforth, S. E.; et al. Comparing Molecular Photofragmentation Dynamics in the Gas and Liquid Phases. *Phys. Chem. Chem. Phys.* **2013**, *15*, 6567–6582.

Figure Captions

Figure 1. Representative transient absorption spectra of a 60 mM solution of NMP in CH_3CN following excitation at 267 nm and probing (a) in the UV/visible region (350-625 nm), and in the mid IR between (b) 1520-1720 cm^{-1} and (c) 2050-2150 cm^{-1} at various pump/probe time delays.

Figure 2. Representative transient absorption spectra of a 60 mM solution of NMP in CH_3CN following excitation at 330 nm and probing (a) in the UV/visible region (350-625 nm), and in the mid IR between (b) 1520-1720 cm^{-1} and (c) 2050-2150 cm^{-1} at various pump/probe time delays.

Figure 3. Time-dependent populations of (a) NMP(S_1) and NMP(S_0) and (b) ketene1 and ketene2, following excitation at 330 nm. The kinetic traces for NMP(S_1) and NMP(S_0) were obtained by numerical integration over, respectively, the 450-500 nm range of figure 2(a) and the 1655-1675 cm^{-1} range of figure 2(b). The kinetic traces in panel (b) were obtained by the decomposition procedure detailed in the SI. The solid and dashed lines are fits to kinetic schemes A and B, respectively.

Figure 4. Kinetic traces extracted for (a) NMP(S_1) and NMP(S_0), and (b) ketene1($v>0$), ketene1 and ketene2 following λ_{Pump}=267 nm. The kinetic trace for NMP(S_1) was obtained by numerical integration over the 450-500 nm range in figures 1(a), with all other kinetic traces obtained by the decomposition procedure detailed in the SI. The solid lines are fits to kinetic scheme A described in the text. Panel (b) is displayed with a split

time-axis to highlight the rapid decay of the ketene1(v>0) signal.

Figure 5. Potential energy curves along the LIIC reaction path for the S_0 and S_1 states of NMP along with the calculated structures at the NMP(S_0) equilibrium geometry and at the S_1/S_0 conical intersection. Possible structures for ketene1 and ketene2 are shown below the potentials.

Figure 1.

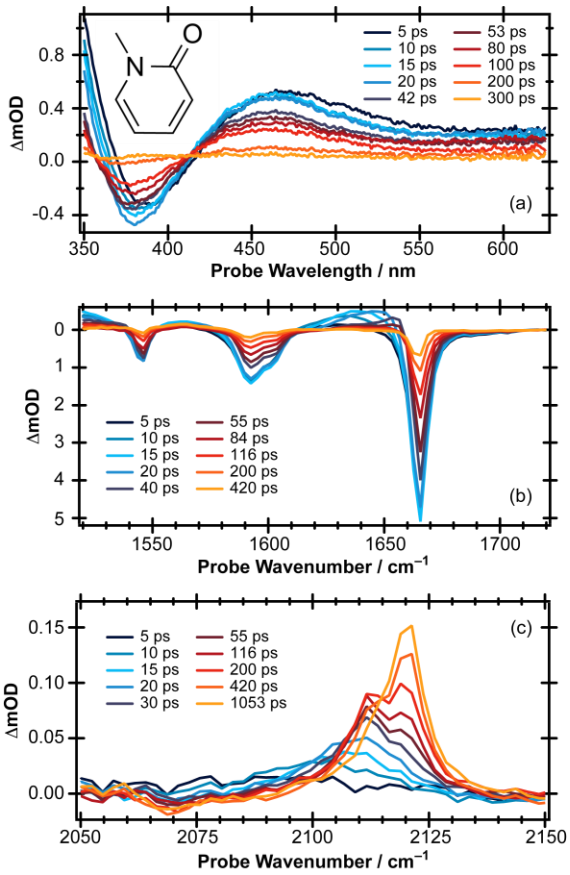
O
N
5 ps
10 ps
15 ps
20 ps
42 ps
53 ps
80 ps
100 ps
200 ps
300 ps
(a)
ΔmOD
Probe Wavelength / nm
5 ps
10 ps
15 ps
20 ps
40 ps
55 ps
84 ps
116 ps
200 ps
420 ps
(b)
ΔmOD
Probe Wavenumber / cm−1
5 ps
10 ps
15 ps
20 ps
30 ps
55 ps
116 ps
200 ps
420 ps
1053 ps
(c)
ΔmOD
Probe Wavenumber / cm−1

Figure 2.

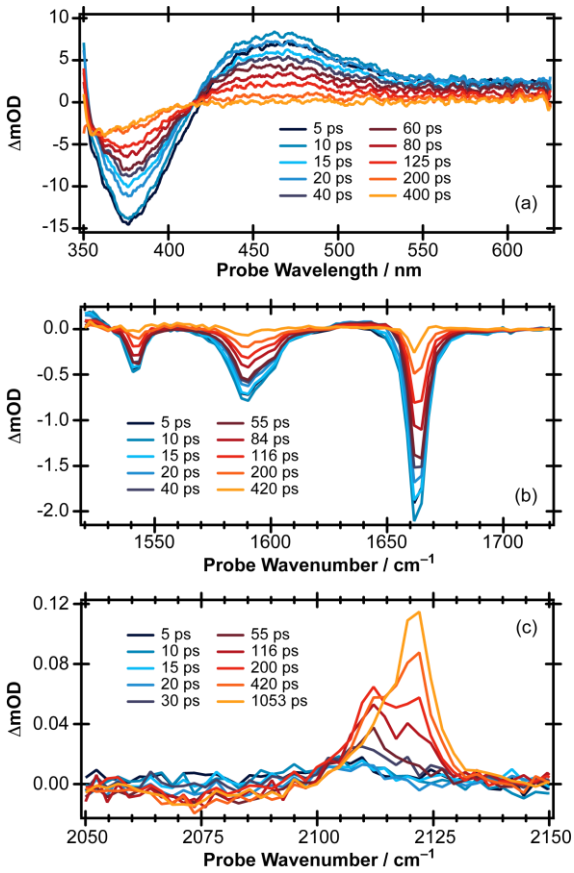
ΔmOD
Probe Wavelength / nm
5 ps
10 ps
15 ps
20 ps
40 ps
60 ps
80 ps
125 ps
200 ps
400 ps
(a)
Probe Wavenumber / cm−1
55 ps
84 ps
116 ps
200 ps
420 ps
(b)
30 ps
1053 ps
(c)

Figure 3.

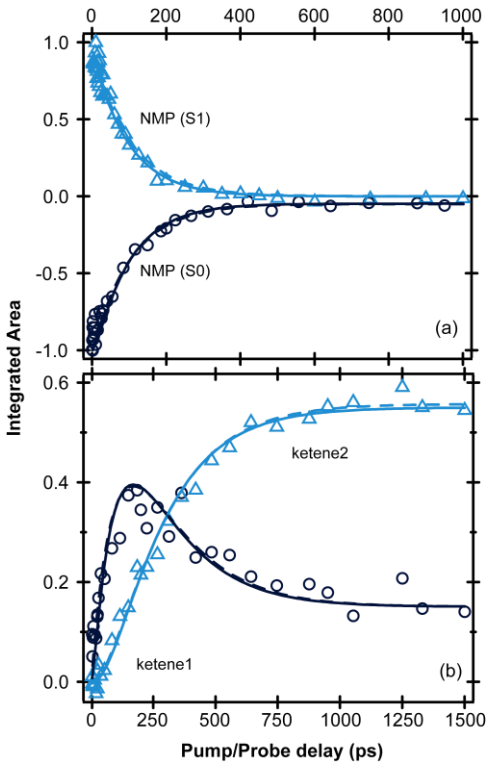
0
200
400
600
800
1000
1.0
0.5
0.0
-0.5
-1.0
NMP (S1)
NMP (S0)
(a)
Integrated Area
0.6
0.4
0.2
0.0
ketene2
ketene1
(b)
0
250
500
750
1000
1250
1500
Pump/Probe delay (ps)

Figure 4.

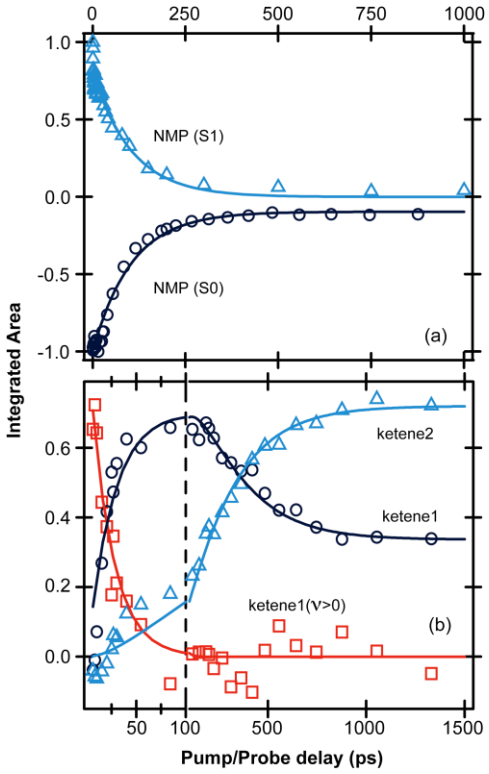
0
250
500
750
1000
1.0
0.5
0.0
-0.5
-1.0
NMP (S1)
NMP (S0)
(a)
Integrated Area
0.6
0.4
0.2
0.0
ketene2
ketene1
ketene1(v>0)
(b)
50
100
500
1000
1500
Pump/Probe delay (ps)

Figure 5.

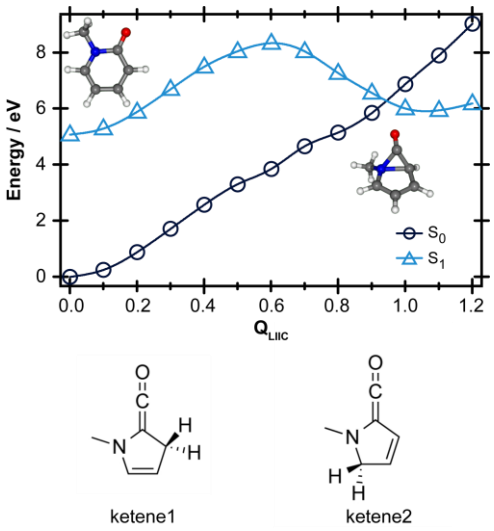
Energy / eV
0
2
4
6
8
0.0
0.2
0.4
0.6
0.8
1.0
1.2
Q_{LIIC}
S_0
S_1
O
C
N
H
H
ketene1
O
C
N
H
H
ketene2

Table 1. Rate coefficients, time constants, and their one-standard deviation uncertainties determined for the photo-initiated rearrangements of NMP assuming kinetic scheme A.

Rate coefficient	Value (ps^{-1})	Time constant	Value (ps)
k_1[a]	2.7	τ_1	0.37
k_2[a]	0.135	τ_2	7.41
k_3	0.045(4)	τ_3	22(2)
k_4 (330 nm)	0.0039(2)	τ_4 (330 nm)	256(13)
k_5 (330 nm)	0.00105(9)	τ_5 (330 nm)	952(82)
k_4 (267 nm)	0.0032(2)	τ_4 (267 nm)	313(20)
k_5 (267 nm)	0.0015(2)	τ_5 (267 nm)	667(89)
k_6	0.00049(9)	τ_6	2040(375)
k_7	0.0091(3)	τ_7	110(4)

[a] k_1 and k_2 are fixed at these values. See text for details.

Table 2. Rate coefficients, time constants, and their one standard deviation uncertainties determined for the photo-initiated rearrangement of NMP at λ_{Pump} = 330 nm assuming kinetic scheme B.

Rate coefficient	Value (ps^{-1})	Time constant	Value (ps)
$k_{7'}$	0.0104(5)	$\tau_{7'}$	96(5)
$k_{8'}$	0.005(1)	$\tau_{8'}$	200(40)
$k_{4'}$	0.0040(2)	$\tau_{4'}$	250(13)
$k_{5'}$	0.0011(1)	$\tau_{5'}$	909(83)
$k_{9'}$[a]	0.1	$\tau_{9'}$	10

[a] $k_{9'}$ fixed at this value, see text for details